Synchrotron X-ray Fluorescence Study on Chloride-induced Stress Corrosion Cracking in Austenitic Stainless Steel Welds

Seunghyun Kim [a*], Gidong Kim [a], Kangwoo Ahn [b], Jun Lim [b], Sang Woo Song [a]
[a]Joining Technology Department, Korea Institute of Materials Science, 797 Changwondae-ro, Changwon-si 51508
[b] Pohang Accelerator Laboratory, 80 Jigok-ro, 127beon-gil, Nam-gu, Pohang-si, 37673
[*]*Corresponding author: skims@kims.re.kr*

1. Introduction

Chloride-induced stress corrosion cracking (CISCC) is degradation phenomenon that generally reported in sea-shore structures including dry storage canister [1]. Combination effects of corrosive environment, materials susceptibility and residual stress initiate and stimulate CISCC in austenitic stainless steels. Some studies have suggested mechanism and mitigation techniques for CISCC but still in debate [2].

Prior works on CISCC behavior of welds have found that ferrite and austenite boundary is susceptible to CISCC due to localized galvanic effects [3]. However, the nature of CISCC by the galvanic coupling between phases or constitute should be further investigated since its complexity. In this study, synchrotron X-ray and multiple lab-scale microstructure and chemical analysis instruments are exploited to investigate CISCC behavior in austenitic stainless steel welds. Even though synchrotron X-ray imaging is state-of-the-art materials characterization technique, its application in nuclear and corrosion society is in early stage [4]. Thus, it is expected that it would expand the view on fundamental mechanism of CISCC.

2. Methods and Results

2.1 Preparation of Materials

Austenitic stainless steel welds, 304L-ER308L and 316L-ER316L, were prepared by gas tungsten arc weld (GTAW). And they were cut and manufactured in U-bend shape. To prohibit galvanic coupling between the specimen and structures, polytetrafluorethylene (PTFE) washers were installed (Fig. 1).

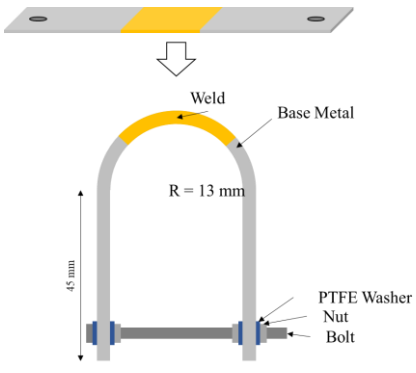

Fig. 1. Geometry of a U-bend specimen

2.2 CISCC Tests

CISCC tests of the prepared U-bend specimen were conducted in a cyclic corrosion chamber which is able to adjust temperature and RH and spray salt solution. Temperature and RH of the test condition was 60°C, 30%RH, respectively. As enlisted in Table 1, the tests were carried out in multiple steps: Step 1 for initial conditioning of temperature and RH; Step 2 for initial salt deposition; Step 3 for maintaining temperature and RH for 10 hrs; and Step 4 for salt spray for 0.5 hrs. As shown in Fig. 3, each test was composed of Step 1 – Step 2 – (Step 3 – Step 4) – (Step 3 – Step 4) –… for 3 months. During the Step 4, RH was elevated due to supply of moisture into the chamber but it was stabilized within 10 min.

Table I: CISCC test steps

Step	Condition	Duration
1	T = 60°C, RH = 30 %	5 hrs
2	Spray 3.5 wt% NaCl	1 hr
3	T = 60°C, RH = 30 %	10 hrs
4	Spray 3.5 wt.% NaCl	0.5 hr

2.3 Microstructure and Chemical Analysis

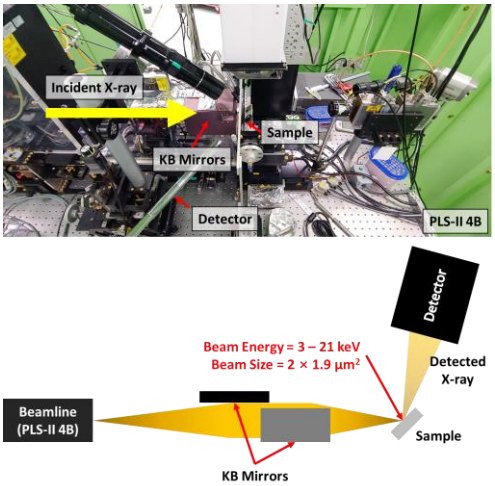

Fig. 2. Photography and schematic diagram of PLS-II 4B beamline

Microstructure and chemical analysis on the CISCC morphologies were also carried out using scanning electron microscope (SEM), transmission electron microscope (TEM), and electron probe microanalysis (EPMA). Manufacturing of TEM samples was carried out using focused ion beam. Synchrotron X-ray fluorescence (SXRF) imaging experiments were carried out in Pohang Light Source – II (PLS-II) 4B beamline. The photography and configuration of the beamline is given in Fig. 2. Incident X-ray from the synchrotron, with energy range 3-21 keV and beam intensity 1.1 × 10^9 photons/sec, was focused using Kirkpatrick-Baez (KB) mirror to achieve micro-sized X-ray (2 μm (H) × 1.9 μm (V) with intensity 6.6 × 10^{11} photons/sec). A detector, which was positioned in 45 ºC against incident X-ray direction, detected fluorescent X-ray from the sample. To achieve 2D SXRF imaging, motors shifted a sample in both X- and Y-direction.

2.4 Results and Discussion

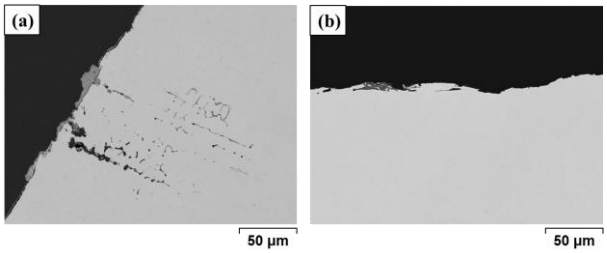

Fig. 3. SEM images on morphologies of (a) CISCC in 304L-ER308L and (b) pitting corrosion in 316L-ER316L

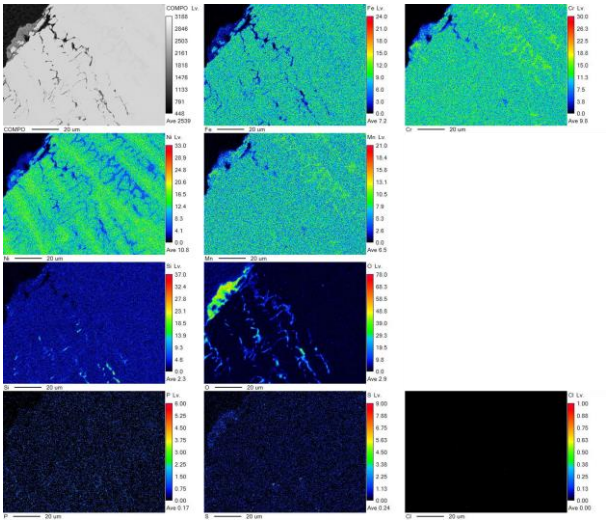

Fig. 4. EPMA images on CISCC region in 304L-ER308L

As shown in Fig. 3, after 3 months of immersion, CISCC occurs only in 304L-ER308L. CISCC propagates in ferrite region meaning ferrite is susceptible to CISCC [5]. EPMA result (Fig. 4) gives that propagation of CISCC along with ferrite is due to Cr and Ni contents in ferrite and austenite. Since Cr and Ni is ferrite and austenite former, respectively, enrichment of Ni in austenite induces relative Ni depletion of Ni in ferrite. Since Ni is corrosive resistive alloy elements in chloride-containing media, selective corrosion in ferrite occurs.

TEM images (Fig. 5) on CISCC region in 304L-ER308L also gives that CISCC propagation occurs due to selective corrosion in ferrite according to depletion of Ni and diffraction pattern analysis in region C.

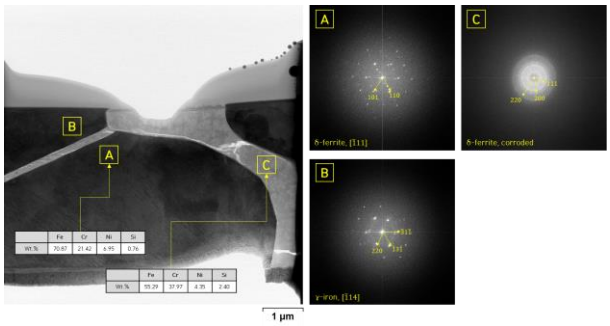

Fig. 5. TEM images on CISCC region in 304L-ER308L

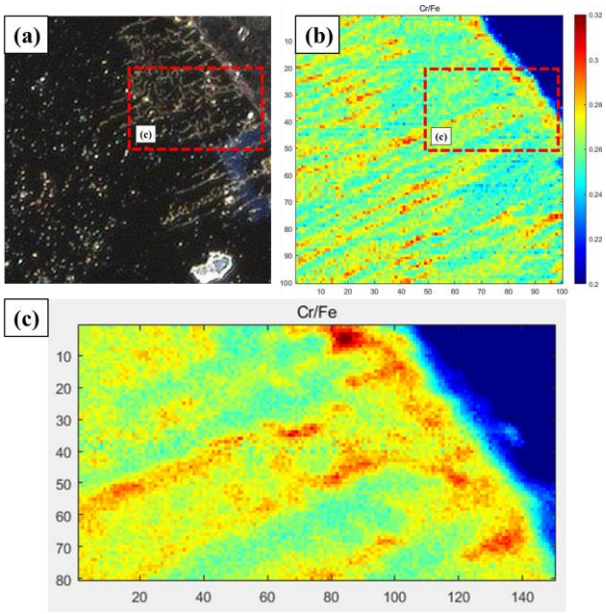

Fig. 6. SXRF images on 304L-ER308L: (a) optical microscope images for (b) and (c), (b, c) SXRF mapping images on Cr/Fe ratio

SXRF images obtained in PLS-II 4B beamline is given in Fig. 6. To investigate selective corrosion in ferrite, Cr/Fe ratio map is illustrated. Where ferrite exists, Cr/Fe ratio is higher than austenite matrix. However, corroded ferrite region gives low Cr/Fe ratio. This is due to Cr depletion during CISCC propagates.

3. Conclusions

CISCC is a potential threat hindering structural and materials integrity of dry storage canister especially for austenitic stainless steel. Ferrite is known as to be susceptible to CISCC due to its electrochemical properties so SXRF is exploited to investigate its nature. SEM, TEM, EPMA and SXRF results give that

selective corrosion in ferrite and it is CISCC propagation site.

REFERENCES

[1] R.L. Sindelar, B.L. Garcia-diaz, J.T. Carter, A.J. Duncan, CHLORIDE-INDUCED STRESS CORROSION CRACK GROWTH UNDER DRY SALT CONDITIONS – APPLICATION TO EVALUATE GROWTH RATES IN MULTIPURPOSE CANISTERS, Proc. ASME 2016 Press. Vessel. Pip. Conf. (2016) 1–7.

[2] H.-G. Park, K.-H. Park, Review of Research on Chloride-Induced Stress Corrosion Cracking of Dry Storage Canisters in the United States, J. Nucl. Fuel Cycle Waste Technol. 16 (2018) 455–472. https://doi.org/10.7733/jnfcwt.2018.16.4.455.

[3] M.A. Melia, H.D.A. Nguyen, J.M. Rodelas, E.J. Schindelholz, Corrosion properties of 304L stainless steel made by directed energy deposition additive manufacturing, Corros. Sci. 152 (2019) 20–30. https://doi.org/10.1016/j.corsci.2019.02.029.

[4] K. Tsuji, T. Matsuno, Y. Takimoto, M. Yamanashi, N. Kometani, Y.C. Sasaki, T. Hasegawa, S. Kato, T. Yamada, T. Shoji, N. Kawahara, New developments of X-ray fluorescence imaging techniques in laboratory, Spectrochim. Acta - Part B At. Spectrosc. 113 (2015) 43–53. https://doi.org/10.1016/j.sab.2015.09.001.

[5] G. Sui, E.A. Charles, J. Congleton, The effect of delta-ferrite content on the stress corrosion cracking of austenitic stainless steels in a sulphate solution, Corros. Sci. 38 (1996) 687–703. https://doi.org/10.1016/0010-938X(96)00159-X.